DYNAMIC STRAIN ON THIN DIAPHRAGMS OF A MERCURY TARGET DURING 800-MeV PROTON THERMAL SHOCK TESTS

C. C. Tsai, S. W. Allison, J. B. Andriulli, M. R. Cates, D. D. Earl,
J. R. Haines, F. X. Morrissey, and S. Wender*

*Los Alamos National Laboratory

Prepared by the
Oak Ridge National Laboratory
P.O. Box 2008
Oak Ridge, TN 37831

Managed by
LOCKHEED MARTIN ENERGY RESEARCH CORP.
for the
U.S. DEPARTMENT OF ENERGY
under contract DE-AC05-96OR22464

DYNAMIC STRAIN ON THIN DIAPHRAGMS OF A MERCURY TARGET DURING 800-MeV PROTON THERMAL SHOCK TESTS

C. C. Tsai, S. W. Allison, J. B. Andriulli, M. R. Cates,
D. D. Earl, J. R. Haines, and F. X. Morrissey
Oak Ridge National Laboratory
P.O. Box 2008
Oak Ridge, TN 37831
(423) 574-1124

S. Wender
Los Alamos National Laboratory
P.O. Box 1663
Los Alamos, NM 87545
(505) 667-1344

ABSTRACT

Extrinsic Fabry-Perot Interferometric fiber optic sensors were used to measure dynamic strains on thin diaphragms of a liquid mercury target, which was subjected to intense 800-MeV proton thermal shock tests. The mercury target is engineered with very thin end plates or diaphragms (either 0.6 mm or 1.9 mm) for studying large strain effects. During thermal shock tests, the mercury in the target interacted with an intense pulsed beam of 2.4×10^{13} protons. The resulting pressure waves lead to large strains exceeding 250 microstrains on a 0.6-mm diaphragm. Significant factors relative to the accuracy of strain measurements are emphasized, such as the sensor air gap, alignment of sensors, and frequency response of the strain instrument. In this paper, dynamic strains measured on thin diaphragms are described and discussed.

I. INTRODUCTION

The proposed Spallation Neutron Source (SNS) project is an accelerator-based pulsed neutron scattering research facility. This facility offers new opportunities for science research to scientists and engineers in the United States. Neutrons will be produced via spallation reactions in a target material following high-energy proton bombardment. Experiments with neutrons are expected to greatly advance the knowledge of materials and development of new products to boost the American economy in the 21st century.

Mercury has been chosen as the SNS neutron production target material;[1] it is expected to withstand thermal shock loads of intense proton beam impact and produce neutrons with high brightness and good efficiency. However, several important design issues must be resolved in developing an SNS mercury target feasible for handling intense proton beams at power levels of 2 MW. At this power level, the pulsed beam parameters are designed to be 1000-MeV proton energy, 2-mA average current, ~0.6-μs pulse width, and 60-cycles/s repetition rate (or $\sim 2 \times 10^{14}$ protons per pulse). The thermal shock loads (33,000 J) cause an enormous rate of temperature rise ($\sim 10^7$ °C/s) in mercury, or on the order of 10°C temperature rise per beam pulse in the mercury. The thermal-shock-induced pressure waves in liquid mercury could lead to large, cyclic stresses in vessel walls of the mercury target and, thus, limit the target lifetime. For such thermal shock applications, one of the key design efforts is to extend the lifetime for the thin target vessel.

To address these design concerns, thermal shock tests on mercury targets[2–5] have been conducted at high-energy accelerator facilities at both the Brookhaven National Laboratory (BNL) and the Los Alamos National Laboratory (LANL) since 1997. Those tests were successful in demonstrating the usefulness of instrumentation using fiber optic sensors to measure dynamic strains of the target vessel in intense radiation environments. The objectives of such tests were to collect experimental data for initial comparison with predictions made by state-of-art thermal shock physics codes.[6–8] Benchmarking these codes or understanding how the thermal shock phenomena scales is critical to validate the SNS target design and development.

Recently, two types of mercury targets (A and B)[9] were designed to simulate SNS targets. These target vessels were made of 316 type stainless steel (SS) sheets. Target A was fabricated by attaching a 10-cm-diam dome to a cylinder (10-cm diameter and 15 cm long). Target B was fabricated by using two thin end plates to enclose a small target volume (5-cm diameter and 5 cm long). These sample targets were used for thermal shock tests at the Los Alamos Neutron Science Center–Weapon Neutron Research (LANSCE-WNR) beam facility. By selecting an

appropriate beam size of 3- to 4-cm diameter and various beam intensities up to ~2.4 × 10^{13} protons per pulse (~0.3 μs), the beam-induced pressure waves in mercury of these sample targets were of the same magnitude as expected in the SNS target. The accelerator facility was operated to provide beams with various power levels (full, one-half, or one-quarter). During the thermal shock experiments on Target A, target strains were measured by using Extrinsic Fabry-Perot Interferometric (EFPI) strain gages, and mercury pressures were measured by fiber optic pressure sensors. Valuable data from vessel strains and mercury pressures of Target A were collected, analyzed, and published in the proceedings of this meeting.[10–11]

To study large strain effects, very thin SS diaphragms of Target B were tested by using a single pulsed proton beam to provide thermal shock exposure. Dynamic strain data were recorded for three single-pulse beam shots. The experimental setup and significant results are reported and discussed in this paper.

II. EXPERIMENTAL SETUP

Figure 1(a) shows a sketch of Target B that was designed and fabricated with thick side walls (50.8 mm) and thin end plates (either 0.6-mm- or 1.9-mm-thick 316 type SS diaphragms). This target has a small cylindrical target volume (50.8 mm in length and 50.8-mm inside diameter) that is loaded with mercury. On the target cylinder, three supporting tabs were used to suspend the target on a supporting frame. Such a target allows the thin diaphragms to respond dynamically to the thermal shock beam impact.

The thin end plates are expected to have large strains under the intense proton thermal shock loading and associated pressure waves in the mercury. For investigating potential plate deformation, each thin plate was prepared by using a diamond turning lathe to machine concentric circles of 10-μm-deep grooves that have a 5-mm radius increment. (The deformation measurements for these plates after their exposure to beam pulses will be discussed in Section IV.) On each plate, two fiber optic strain gages [as shown in Fig. 1(b), No. 1 at the center and No. 2 at 5 mm away] were installed for measuring dynamic strains. The significant parameters of these strain gages are listed in Table 1; for example, on the 0.6-mm-thick plate, the strain gage SN#A1 had an air gap of ~75 μm, a gage length of 19.12 mm, and a calibrated peak-to-peak voltage of 2.5 V.

To prevent accidental leakage of mercury vapor into the LANSCE-WNR facility, the mercury target was installed inside a secondary SS container. The secondary container was designed so that any mercury from the target is fully contained in a region below the beam strike point. During thermal shock tests, the secondary container was

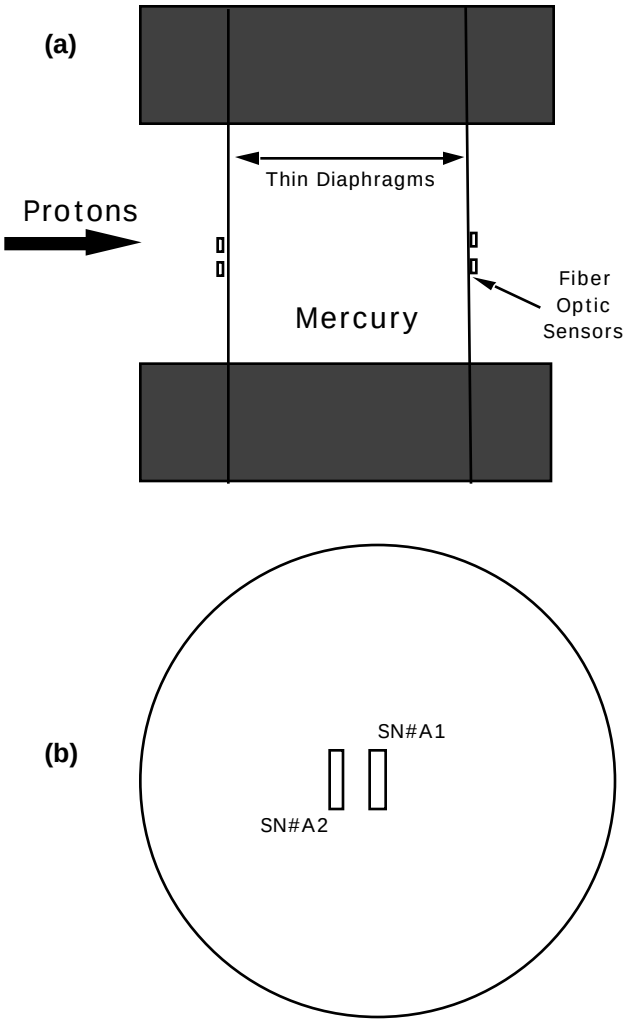

Figure 1. Schematic drawings of (a) Target B assembly and (b) location of fiber optic sensors SN#A1 and SN#A2 on each diaphragm.

Table 1. Significant parameters of strain gages

Strain gage	Air gap (μm)	Gage length (mm)	Peak-to-peak voltage (V)	Peak strains
SN#A1	74	19.12	2.5	266
SN#A2	68	16.86	1.9	260
SN#F1	53	18.13	4.6	202
SN#F2	57	15.84	2.7	196

placed on a lift table that can be moved up or down for aligning the target center to the beam.

As published elsewhere,[2–5] EFPI fiber optic strain sensors were demonstrated to be viable strain gages for measuring dynamic strains of a target vessel in an intense radiation background. An EFPI strain sensor consists of a single-mode input/output (I/O) optical fiber, a multimode reflector optical fiber, and an air gap between the fibers in a silica capillary tube. The sensor was installed on a target vessel by attaching its I/O optical fiber and its reflector optical fiber with epoxy-based adhesives. The distance between the glued spots is called the gage factor or gage length. The air gap changes in the EFPI sensor equal to the changes of the gage length. Capable of measuring the air gap optically, the EFPI strain sensors work well as dynamic strain gages.

The air gap displacement in an EFPI sensor is measured by laser light from a fiber optic support system (FOSS I),[12] a product of F&S, Inc. A laser diode in the FOSS I generates light with a wavelength of 1310-nm, which is launched into the I/O fiber of an EFPI sensor. The reflected laser light from the I/O optical fiber at the air–glass interface, is the reference signal. The reflected light from the reflector fiber is the sensing signal. These two reflected light waves interfere with each other in the single-mode I/O fiber and yield a classic interferometric signal, which is converted into an electrical analog output signal via photodiode, amplifiers, and other electronics in the FOSS I unit. The typical output voltage signal is sinusoidal with its phase angle corresponding to the air gap changes in the sensor. Each period represents one optical fringe and is equivalent to an air gap change of half the laser wavelength (655 nm). With a typical gage length of 20 mm, the strain gage measures 32.8 microstrains per fringe.

The mercury target was positioned in Target 2 (Blue Room area) of the LANSCE-WNR facility, 40 m away from the strain measurement electronics. Figure 2 shows a schematic block diagram of a strain measurement system. In addition to EFPI sensors on a mercury target, the system includes 40 m fiber optic cables, FOSS I units, a digital scope, and a personal computer (PC). Each channel of a FOSS I unit is used to measure air gap changes in an EFPI sensor, thus the dynamic strain signals. The digital scope is used to acquire transient raw strain signals, and the PC is used to record and store the raw strain signals in a PC file for further analysis.

When a single-pulse proton beam impacted Target B, the induced pressure waves in mercury caused large strains on the thin diaphragms. The associated air gap changes in the strain gages were monitored and acquired. The digital scope was triggered by a beam pulse signal, and set up to record raw strain signals for 10 to 50 ms at sampling rates variable up to 10 mega-samples per second. If the dynamic strain was a partial fringe (and monotonic), the PC data acquisition system analyzed and displayed the measured transient strains.[2–5]

Strain (in microstrain) = (partial fringe)
× 655 (μm)/gage length (mm) . (1)

Here,

Partial fringe = signal (mV)/peak-to-peak voltage(mV) . (2)

However, for a case with large strains (or signals having multiple fringes), the number of fringes between turnaround points were determined from a plot of the strain raw data. The following formula are used to determine strains.

Strain (in microstrain) = (number of fringes)
× 655 (μm)/gage length (mm) . (3)

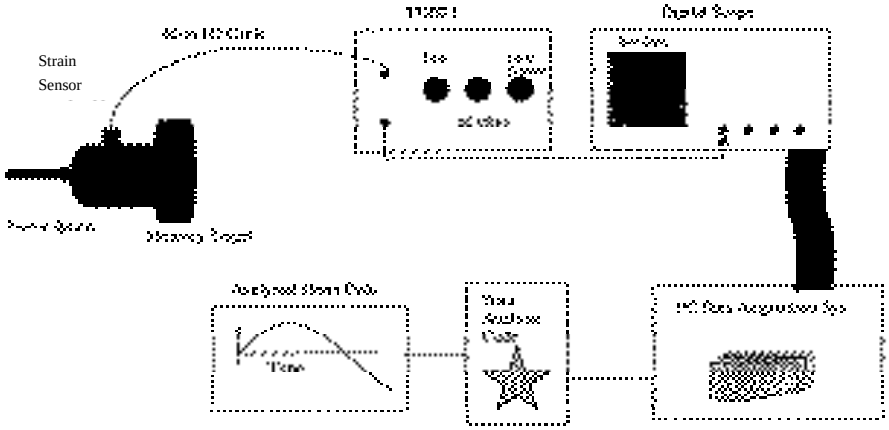

Figure 2. Schematic block diagram of strain measurement system.

III. DYNAMIC STRAIN MEASUREMENT

Dynamic strain measurements on thin diaphragms of the mercury Target B were done by impact of a single-pulse intense beam of 2.4×10^{13} protons at 800 MeV. For 0.6-mm-thick end plates, the thermal shock test was conducted for one beam shot. For 1.9-mm-thick end plates, the thermal shock tests were done for two beam shots. After each beam impact, the analog voltage output of a FOSS I unit was acquired and recorded on the digital scope as raw strain voltage signals of a strain gage, as shown in Fig. 2. Such raw strain signals were subsequently transferred and stored in a PC file and further analyzed. The characteristics of raw voltage signals and analyzed strains so obtained are elaborated in the following sections.

A. Raw Strain on 0.6-mm Diaphragm

Figures 3(a) and 3(b) are raw voltage data measured from strain gages SN#A1 and SN#A2, respectively. The

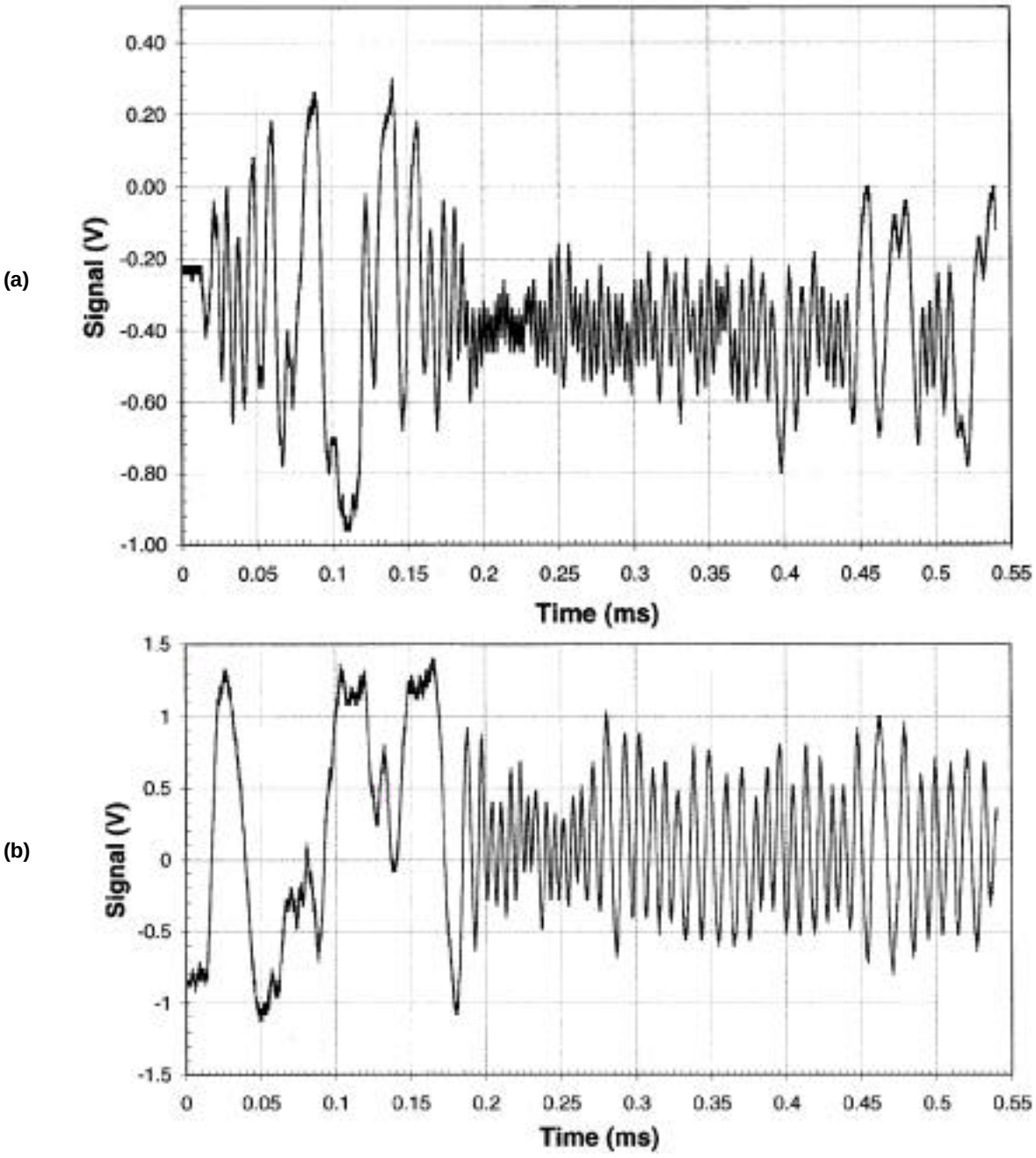

Figure 3. Traces of raw strain data: (a) for SN#A1 and (b) for SN#A2.

gage SN#A1 was installed at the center of a 0.6-mm diaphragm, and SN#A2 was at 5 mm from the center. After the trigger, the impact time of the beam pulse on the target is ~10 μs; in these figures, the raw signal appeared at ~13 μs. The amplitude of signal trace in Fig. 3(a) increases to a maximum of ~1.2 V at ~100 μs, decreases to a minimum of ~0.08 V at ~225 μs, and fluctuates with slight variations after 225 μs. The peak-to-peak amplitudes in Fig. 3(a) for SN#A1 are always smaller than the calibration values of 2.5 V. Figure 3(b) shows raw strain signals for the strain gage SN#A2. Compared to the gage SN#A1, the gage SN#A2 has a smaller air gap and larger peak-to-peak amplitudes of raw signals. The amplitude of 2.4 V within 200 μs is larger than the calibration value of 1.9 V. After 200 μs, the variations of raw signals are similar to those for the gage SN#A1.

B. Raw Strain on 1.9-mm Diaphragm

Raw voltage data for strain gages SN#F1 and SN#F2 on a 1.9-mm SS end plate are shown on Fig. 4. The temporal variations of these voltage signal traces are very

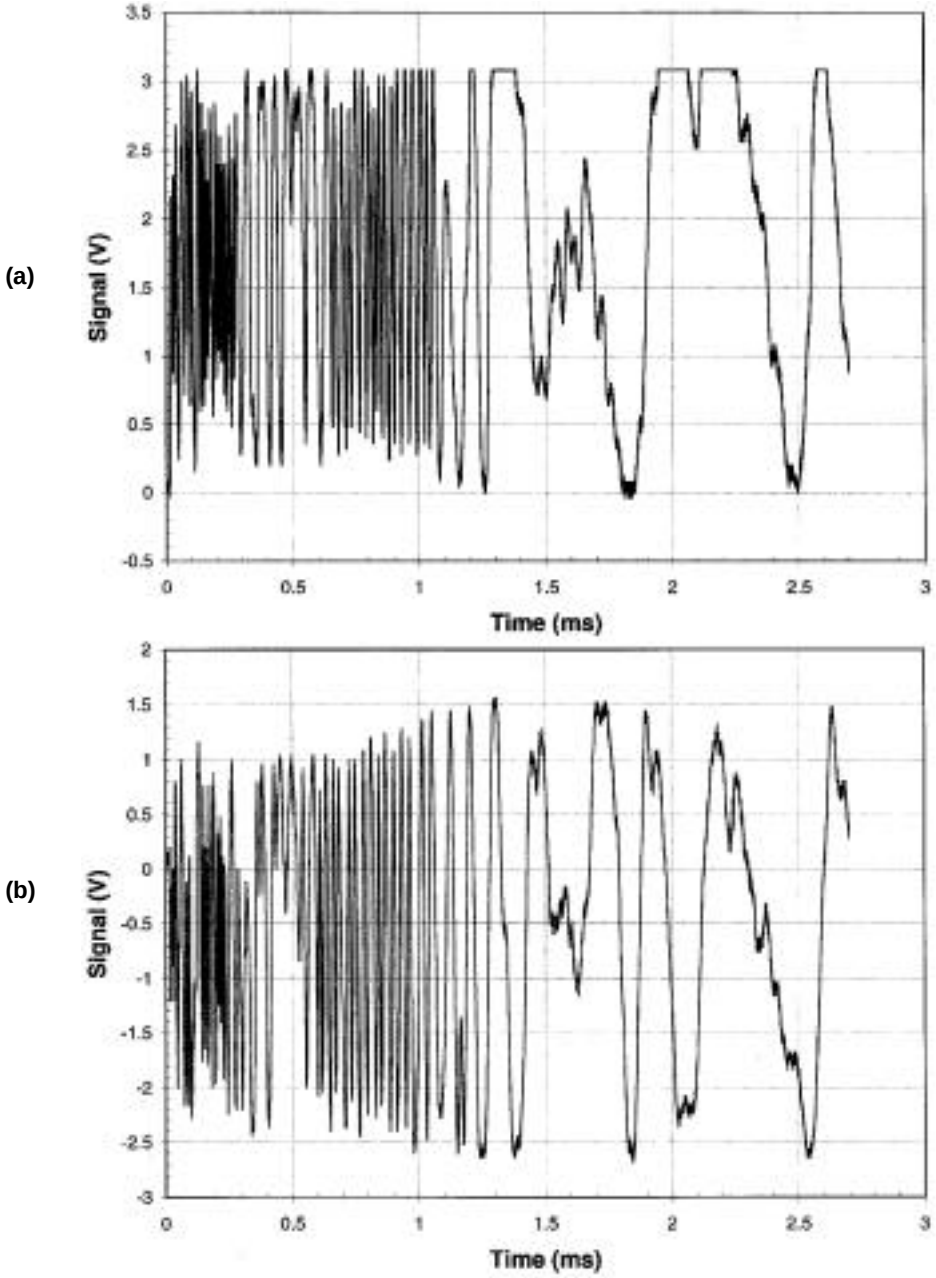

Figure 4. Raw strain data: (a) for SN#F1 and (b) for SN#F2 on a 1.9 SS plate.

similar to each other in both the amplitude and the frequency response. Within the first 300 μs, the raw signal amplitudes are smaller than the calibration values. The raw signals oscillate at lower frequencies between 300 μs and 600 μs and at higher frequencies from 600 μs to 1.1 ms. After 1.1 ms, the raw signal amplitudes increase and approach the calibration values. Such dynamic features of raw signal amplitudes could be associated with the dynamic response of diaphragms to the thermal-shock-induced pressure waves in liquid mercury of the target vessel.

C. Strain Analysis

Under the impact of each intense beam pulse of 2.4×10^{13} protons at 800 MeV, the thermal-shock-induced pressure waves in liquid mercury subsequently caused large strains on the thin plates of Target B. The pressure waves take 33 μs to travel between the end pates (~5 cm). Raw strain voltage signals will be modulated by such pressure waves at tens of kilohertz. The frequency response of the FOSS I system is rated at 100 kHz. The FOSS I frequency response is inversely proportional to frequency because of the decrease in signal gain at a higher frequency. As reported previously,[3] the output voltages for various frequencies are 100% at 20 kHz, 83% at 50 kHz, 60% at 100 kHz, 50% at 150 kHz, and 44% at 200 kHz. To accurately measure strain values, it is necessary to correct the gain amplitude dependence on signal frequency. Such frequency effects modify acquired waveform or raw strain signals. For example, measured peak-to-peak amplitudes of high-frequency strain signals could be smaller than the calibration values. Such frequency effects need to be taken into account for accurately measuring strain values.

In addition to frequency effects, the acquired waveform of a gage could be affected by the diaphragm curvatures. If the gage SN#A1 were installed on a thin diaphragm with slightly concave surfaces, the plate could be expanded and flattened out by the beam-induced pressures, and the air gap of the gage could be decreased with an improved alignment of optic fibers. These changes in the air gap and alignment could lead to increases of the raw signal amplitudes, as shown by the waveform from ~13 μs to ~100 μs in Figure 3(a). After ~100 μs, the thin plate could start to contract to concave shape, the corresponding increases in the air gap and degrading alignment could lead to the decrease of signal amplitudes. If the concave plate causes very poor alignment, the gage could operate outside the linear range and yield a small signal output, perhaps as that shown at ~225 μs in Figure 3(a). The acquired waveform after ~225 μs shows a series of signal fluctuations that could result from dynamic response of the diaphragm to the mercury pressure waves.

The wavelength of the laser light used in the FOSS I unit is 1310 nm. The gage length for the strain gage SN#A1 is 19.12 mm. The strain for each fringe is 34.26 microstrains. Following the previous discussions on raw strain signals, each sinusoidal period can be considered as a fringe. Considering signal frequency dependence, fringe counting can be used to obtain strain values. In Fig. 3(a) for the gage SN#A1, ~7.5 fringes between ~13 μs and ~100 μs, the measured strain can be as large as 266 microstrains (as listed in the last column of Table 1). The strains on the plate decrease after ~102 μs and approach a minimum at ~206 μs. The analyzed strains so obtained are shown in Fig. 5. Following similar analyzing processes, the peak strain values of other gages

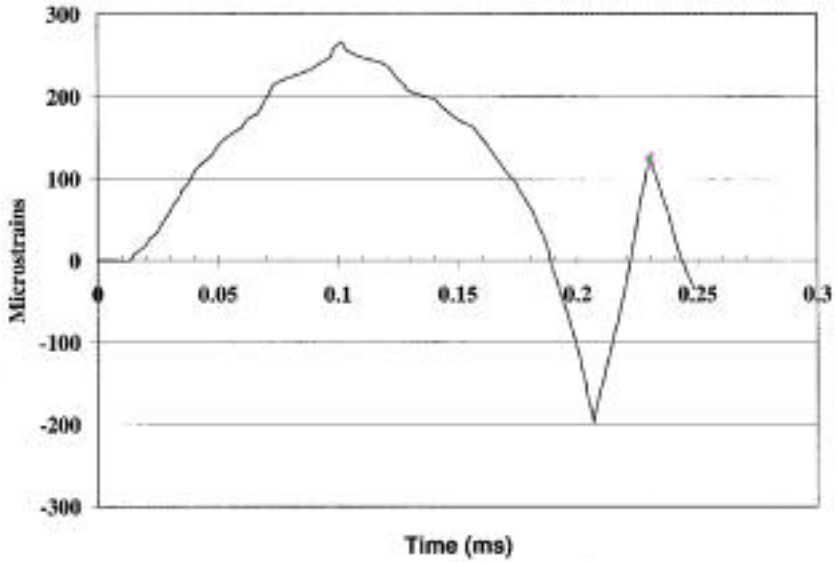

Figure 5. Analyzed strains of SN#A1.

(SNA#2, SN#F1, and SN#F2) are listed in Table 1. The accuracy of this preliminary strain analysis is greatly affected by the turnaround points chosen from the acquired waveform.

The strain analyses of raw data from various strain gages are being refined and will be revised based on the results of ongoing strain analysis of existing data or from the next thermal shock tests using an improved strain measurement system.

IV. DISCUSSION

In addition to measuring dynamic strains, the EFPI fiber optic sensors on diaphragms were also used for measuring long-timescale deformation of diaphragms. The air gap changes of these sensors were measured by a Fiberscan 2000 instrument, a product of F&S, Inc. Measurements on the air gap distance of each sensor were repeated to achieve reproducibility of 0.01 μm or less. For a typical air gap distance of 50 μm, the accuracy is within 0.02%. The air gap of each sensor was measured for three cases: right before the beam pulse, right after the beam impact, and on the next day. The air-gap increase of sensors SN#A1 and SN#A2 on the 0.6-mm diaphragm facing the beam was measured to be ~2 μm right after the beam exposure and ~1.5 μm on the next day. The thermal deformation of diaphragms responding to temperature changes of mercury in the target may explain the air-gap changes from ~2 μm to ~1.5 μm. Thus, ~1.5 μm is estimated to be the permanent deformation over a gage length of 19.12 mm. This is equivalent to ~78 microstrains. It implies a slight permanent deformation (<0.01%) on this thin diaphragm. The air-gap increases of sensors on the other 0.6-mm diaphragm under the same beam exposure were also measured, but were smaller, about 0.18 μm over a gage length of 18.85 mm. It implies a permanent deformation below 0.001%. Such beam-induced deformation measurements were also done on 1.9-mm diaphragms. No definite air-gap changes were measured for sensors on the 1.9-mm diaphragms, implying that such thicker diaphragms are free from plastic deformations under the same beam exposure.

The spacing between each pair of concentric circles of 10-μm-deep groves on each diaphragm was carefully measured in an attempt to measure any permanent deformation. A high-precision diamond tuning lathe was used for such measurements about 1 month after the thermal shock tests. No definite values of permanent deformations were measured for all diaphragms. This measurement uncertainty could be due to insufficient resolution of the measuring instrument, as elaborated below. If a permanent deformation of 0.01% exists on a 0.6-mm diaphragm, the spacing (5 mm) between adjacent concentric circles could have an increment of ~0.5 μm. This small increment in spacing may not be resolved by the high-precision diamond tuning lathe, which only has a fine resolution of 1 μm. Obviously such an instrument is ineffective for measuring such small permanent deformations of diaphragms. But the method using a Fiberscan 2000 instrument for measuring sensor air gap was able to measure such small deformations.

The present strain measurement system measured dynamic strains of ~266 microstrains on a 0.6-mm-thin diaphragm and ~200 microstrains on 1.9-mm diaphragm. Many factors that affect the accuracy of the strain measurement system (Fig. 2) are listed as follows.

1. The thermal shock pressure waves could affect deformation of diaphragms and thus measured strains.
2. Fiber alignment, air gap between fibers, and gage length of strain gages installed on the target vessel or plates could influence amplitudes and frequency response of raw signals, thus, the analyzed strains.
3. Laser current, amplifier gain, direct current (dc) offset, and frequency response of the FOSS I system could affect the accuracy and characteristics of raw signals and the analyzed strains.
4. Sampling rates, analog/digital converter, and record length of the PC data acquisition systems, including digital scope, could affect the accuracy of raw data and, thus, the analyzed strains.
5. Data analysis codes for processing raw strain data could affect the accuracy of measured strains. To improve accuracy, the following additional processes were used in data analysis.
   - Use a plot of raw signals of fiber optic sensor pairs to determine the times of the turnaround points.
   - Determine the number of fringes between turnaround points.

The directional changes of strains on thin plates are difficult to clearly identify on raw strain signals measured by the present FOSS I system. An improved strain instrument should be developed for measuring direction and strains at high frequencies. The frequency response of such a system should be extended above 1 MHz. In addition, data analysis computer codes should be improved for analyzing strain data on-line. Such an improved strain measurement system is being developed for the next sequence of thermal shock tests. Measured strains can be used for validating predictions of theoretical codes, benchmarking the codes for SNS mercury target design, and development.

ACKNOWLEDGMENTS

The authors would like to express their appreciation and thanks to Greg Chaparro, Lloyd Hunt, and accelerator staff members at LANL for their excellent support in providing 800-MeV proton beams for thermal shock tests on mercury targets at the LANSCE-WNR facility. This work has benefited from the use of the LANSCE-WNR facility that is funded by the U.S. Department of Energy under contract W-7405-ENG-36. Research at ORNL was sponsored by the Office of Energy Sciences for the U.S. Department of Energy under contract DE-AC05-96OR22464 with Lockheed Martin Research Corp.

REFERENCES

1. J. R. Haines, T. A. Gabriel, and T. G. McManamy, "Overview of the Target Systems for the Spallation Neutron Source," *Proceedings of AccApp 98,* p. 222 American Nuclear Society, La Grange Park, Illinois (1998).
2. J. R. Haines, D. D. Earl, and C. C. Tsai, "Summary of Mercury Target Thermal Shock Tests Conducted at Accelerator Facilities in FY 1997," SNS/TSR-0041, Lockheed Martin Energy Research Corp., Oak Ridge National Laboratory, December 1998.
3. D. D. Earl, J. R. Haines, and C. C. Tsai, "Measurement of Strain Experienced by a Mercury Target Vessel," SNS/TSR-0040, Lockheed Martin Energy Research Corp., Oak Ridge National Laboratory, December 1998.
4. D. D. Earl, S. W. Allison, C. C. Tsai, and J. R. Haines, "Improved Fiber Optic Pressure and Strain Sensing Techniques for Use in High Radiation Environment," *Proceedings of AccApp 98*, p. 665, American Nuclear Society, La Grange Park, Illinois (1998).
5. C. C. Tsai, D. D. Earl, S. W. Allison, and J. R. Haines, "Dynamic Fiber Optic Sensors Under Intense Radioactive Environments," *Proceedings of AccApp 98*, p. 658, American Nuclear Society, La Grange Park, Illinois (1998).
6. R. P. Taleyarkhan, S. H. Kim, and J. R. Haines, "Modeling and Analysis of AGS Thermal Shock Experiments," *Proceedings of AccApp 98*, p. 670, American Nuclear Society, La Grange Park, Illinois (1998).
7. R. P. Taleyarkhan, S. H. Kim, and J. R. Haines, "Pretest Predictions of Surface Strain and Fluid Pressure in Mercury Targets Undergoing Thermal Shock," *Transactions of the American Nuclear Society*, **80**, 311 (1999).
8. S. H. Kim, R. P. Taleyarkhan, and J. R. Haines, "Thermal Shock Analysis of the BNL/AGS Mercury Target Experiments," *Transactions of the American Nuclear Society*, **80**, p. 312 (1999).
9. C. C. Tsai, J. B. Andriulli, S. W. Allison, M. R. Cates, D. D. Earl, J. R. Haines, F. X. Morrisey, "Dynamic Strain and Pressure Measurements of a Mercury Target Under Thermal Shock Tests," *Transactions of the American Nuclear Society*, **80**, p. 313 (1999).
10. M. R. Cates, D. D. Earl, C. C. Tsai, S. W. Allison, J. R. Haines, F. X. Morrisey, and J. B. Andriulli, "Dynamic Strain on a Mercury Target Vessel During 800-MeV Proton Thermal Shock Tests," in this proceedings.
11. J. B. Andriulli, S. W. Allison, M. R. Cates, D. D. Earl, J. R. Haines, F. X. Morrisey, and C. C. Tsai, "Dynamic pressure of Liquid Mercury Target During 800-MeV Proton Thermal Shock Tests," in this proceedings.
12. S. H. Poland, "Fiber and Sensor Technologies Application Notes: FOSS I Operation and Fringe Counting, Rev. D," March 1997.